JOURNAL OF APPLIED ELECTROCHEMISTRY 22 (1992) 456–463

Impedance parameters of individual electrodes and internal resistance of sealed batteries by a new nondestructive technique

S. A. ILANGOVAN, S. SATHYANARAYANA*

Department of Inorganic and Physical Chemistry, Indian Institute of Science, Bangalore, 560 012, India

Received 11 February 1991; revised 29 August 1991

A new robust method for the nondestructive determination of impedance parameters of the individual electrodes of sealed batteries has been developed. In this method, a battery is discharged at a constant current of about 2000 h (or less) rate for a few seconds only. The discharge transient of voltage against time is analysed theoretically to give effective double layer capacitances and charge transfer resistances of battery cathode and anode separately, as well as the internal resistance of the battery. Experimental data from discharge transients are processed with a new procedure which is immune to normal measurement errors and which permits a resolution of the parameters of the anodic and cathodic relaxation processes even if their time constants are not far apart. The correctness of the method is verified by simulation studies, and applied to sealed recombinant type lead–acid batteries. Diffusion resistance is shown to be negligible under the test conditions. The effects of switching transients and any series inductance are eliminated by the method. The results are directly relevant to improved battery design and failure analysis.

1. Introduction

The expanding role of primary and secondary batteries in modern society has prompted the evolution of a variety of new and improved battery systems in recent years. Sealed batteries especially, which require no maintenance and release no gases or vapours to the environment, are becoming popular. A fundamental characterization of battery operation requires a knowledge of impedance parameters such as charge transfer resistances and double layer capacitances of the cathodes and anodes individually, as well as the internal resistance of the battery. Evaluation of these parameters is particularly difficult with the advent of sealed batteries, since access to the individual electrodes or the electrolyte is impossible without destroying the battery.

In a recent attempt [1] on the 'nondestructive characterization of sealed lead–acid battery cells with electrochemical impedance spectroscopy', several difficulties have been pointed out, and only charge transfer resistances as a sum, as well as double layer capacitances, also as a sum, of anodes and cathodes could be determined.

The problem of nondestructive determination of resistance and reactance parameters of cathodes, anodes as well as the internal resistance *separately* in sealed batteries has not been solved so far. The purpose of this work, therefore, is to offer a solution to the above important problem and demonstrate its application to sealed recombinant lead–acid (SLA) batteries.

* Author to whom all correspondence should be addressed.

2. Theory

2.1. *Description of the model*

The equivalent circuit of a battery may be represented, quite generally, as shown in Fig. 1.

The self-inductances (L_1, L_2; including electrochemical pseudoinductances) in the battery equivalent circuit are often ignored, although there is clear experimental evidence in the literature for their presence [2–5]. Distortion of a.c. impedance plots (capacitive reactance against resistance) is caused by battery self-inductance among other factors. Self-inductance of electrochemical cells is also known in corrosion studies [6] and other cases [7].

The total internal resistance (R_i) of a battery governs the dissipative processes in a battery and is the sum of all the resistive terms in the equivalent circuit of Fig. 1.

$$R_i = R_\Omega + (R_{t,1} + R_{t,2}) + (R_{w,1} + R_{w,2})$$

where $R_\Omega = R_{\Omega,1} + R_{\Omega,2} + R_{\Omega,s}$, and $R_{w,1}$, $R_{w,2}$ are resistive parts of $Z_{w,1}$, $Z_{w,2}$, respectively.

R_i depends on test duration unless the time-dependent diffusion resistances ($R_{w,1}$, $R_{w,2}$) are rendered small by a proper choice of test conditions. In such a case

$$R_i = R_\Omega + R_{t,1} + R_{t,2} \quad (1)$$

Frequently, the *ohmic* component of R_i, namely, R_Ω alone is the quantity sought for as an adequate measure of the battery internal resistance.

The charge transfer resistances ($R_{t,1}$, $R_{t,2}$) are

0021-891X/92

inversely proportional to the exchange current, a fundamental kinetic parameter, for the corresponding reactions at the two electrodes.

The double layer capacitances ($C_{d,1}$, $C_{d,2}$) reflect, primarily, on the effective area available for the charge transfer reactions, an important parameter, at the two electrodes.

In order to obtain the parameters R_Ω, $R_{t,1}$, $R_{t,2}$, $C_{d,1}$ and $C_{d,2}$ nondestructively and individually, test conditions have to be chosen judiciously to eliminate diffusion resistances ($R_{w,1}$, $R_{w,2}$), series inductive reactances due to L_1 and L_2, and to ensure that the change in the state of charge (SOC) of the battery is negligible during the test.

2.2 *Galvanostatic non-destructive test technique*

The above requirements may be met readily with the following galvanostatic nondestructive test (GNDT) conditions.

The battery, initially at equilibrium, is discharged galvanostatically at an extraordinarily low rate (approximately $C/2000$ A were C is the nominal capacity of the battery in Ah) for a duration (usually, a few tens of seconds) not exceeding that when the battery voltage falls by about 2 to 3 mV per cell in the battery. The last condition ensures a linear polarization domain for the battery electrodes which permits considering C_d's and R_t's as constants during the test discharge. The short test duration and the very low rate of discharge imply that the diffusion polarization is negligible compared to charge transfer and ohmic polarization even at the end of the test.* The galvanostatic mode eliminates any contribution by the battery series inductance to the measured voltage change. Finally, the test current and duration ensure that the state of charge of the battery changes by less than 0.01% of the initial value, and that any temperature change caused is less than a few millidegrees at room temperature.

Consistent with the above GNDT test conditions, the equivalent circuit in Fig. 1 can be simplified as shown in Fig. 2.

The voltage response of a battery-cell to discharge under GNDT conditions may be derived readily with reference to Fig. 2, as for example in [9], giving

$$V^r - V = IR_\Omega + IR_{t,1}(1 - e^{-t/\tau_1}) + IR_{t,2}(1 - e^{-t/\tau_2}) \tag{2}$$

* In the linear polarization domain of an electrode, the magnitude of the diffusion polarization is approximately equal to (RT/F) ln $(1 - I/I_L)$ where I_L is the instantaneous limiting current at the given time. Since practical batteries can be discharged at 1 C rate or higher, i.e., for about 3600 s at 1 C rate, the value of I_L above may be taken consecutively as at least 1 C for a test duration of at least about a hundredth of the total duration available at this rate, i.e., for a few tens of seconds. The instantaneous value of I_L could be much higher than what is assumed above, considering the fact that the short circuit currents exceed 20 C rate for charged lead-acid cells [8]. The diffusion polarization, therefore is less than about 26 $(C/2000)/C$ mV or 13 μV at the end of the test, at which time *cell* voltage change is about 2 to 3 mV according to test plan. Diffusion polarization will therefore be only about 13 μV/2.5 mV or about 0.5% at the end of the test. It will be even less than the above at the beginning of the test.

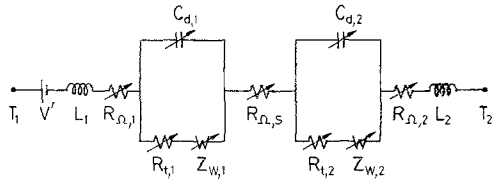

Fig. 1. Generalized equivalent circuit of a battery cell. T_1, T_2: battery terminals; V^r: reversible (equilibrium) e.m.f. of the battery; $R_{\Omega,1}$, $R_{\Omega,2}$: ohmic resistances of cathode (subscript 1) and of anode (subscript 2), for example, due to grid supports, welds, links etc., $R_{\Omega,s}$: ohmic resistance of solution and separator; $R_{t,1}$, $R_{t,2}$: charge transfer resistances of the electrodes; $Z_{w,1}$, $Z_{w,2}$: mass transfer impedances of the electrodes; $C_{d,1}$, $C_{d,2}$: double layer capacitances of the electrodes, L_1, L_2: self-inductances of the electrodes; Arrows indicate possible dependence on cell voltage and state of charge; R_t, Z_w, C_d and L's above represent only the effective values for the porous electrodes in the battery cell since the exact model for the porous structure is unknown. The assignment of subscripts 1 and 2 to cathode and anode is arbitrary.

where V^r is the equilibrium EMF of the cell at the given state of charge, and V is the cell voltage at time t and test current I ($I \geqslant 0$). $\tau_1 = R_{t,1} C_{d,1}$; $\tau_2 = R_{t,2} C_{d,2}$ are the time constants of the charge-transfer controlled processes at the cell cathode and cell anode, respectively. The subscripts 1 and 2 to cathode and anode are assigned arbitrarily.

If the time constants of the two relaxation processes are widely separated, e.g., $\tau_1 \gg \tau_2$, there is no difficulty in solving Equation 2 with experimental data, but such a situation cannot be assumed without adequate reasons as is unlikely to be always valid in practical systems.

2.3. *Algebraic approach*

The general case of comparable (but unequal) time constants is therefore important. Apparently, even in such a case, the desired resistance and capacitance parameters R_Ω, $R_{t,1}$, $R_{t,2}$, $C_{d,1}$ and $C_{d,2}$ may be obtained by solving Equation 2 with experimental V–t data. There are, however, serious difficulties in a direct algebraic (or curve-fitting) procedure in solving the problem, as may be illustrated below.

A typical approach is to take the first four derivatives of V against t at the origin (denoted by the subscript '0'). From Equation 2

$$\begin{aligned}
-\frac{1}{I}\left(\frac{dV}{dt}\right)_0 &= \left(\frac{R_{t,1}}{\tau_1} + \frac{R_{t,2}}{\tau_2}\right) \\
-\frac{1}{I}\left(\frac{d^2V}{dt^2}\right)_0 &= -\left(\frac{R_{t,1}}{\tau_1^2} + \frac{R_{t,2}}{\tau_2^2}\right) \\
-\frac{1}{I}\left(\frac{d^3V}{dt^3}\right)_0 &= \left(\frac{R_{t,1}}{\tau_1^3} + \frac{R_{t,2}}{\tau_2^3}\right) \\
-\frac{1}{I}\left(\frac{d^4V}{dt^4}\right)_0 &= -\left(\frac{R_{t,1}}{\tau_1^4} + \frac{R_{t,2}}{\tau_2^4}\right)
\end{aligned} \tag{3}$$

Denoting the measured values of the l.h.s. terms in Equation 3 as a, b, c and d, respectively, this set of four simultaneous equations may be solved by the usual process of elimination. The result, for example,

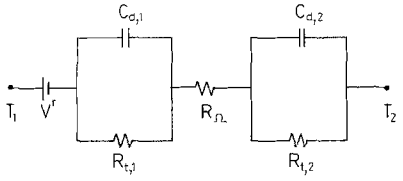

Fig. 2. Equivalent circuit of a battery cell under Galvanostatic NonDestructive Test (GNDT) conditions. Symbols are as in Fig. 1. $(R_{\Omega,1} + R_{\Omega,2} + R_{\Omega,s})$ has been replaced by one series resistance R_Ω.

for τ_1 is

$$d(c^2 - bd)\tau_1^5 + (c^3 - ad^2)\tau_1^4 + 2d(b^2 - ac)\tau_1^3 - 2a(c^2 - bd)\tau_1^2 + (a^2d - b^3)\tau_1 - a(b^2 - ac) = 0 \quad (4)$$

Assuming that a numerical solution of Equation 4 is attempted, it follows that, depending on the signs of the coefficients of the six terms in Equation 4, either one, two, three or five positive real roots will occur for τ_1. In practice, changes in the signs of these coefficients are likely to occur due to inevitable measurement errors such as from switching transients, inaccurate calibrations, inaccurate estimation of derivatives, fluctuations in voltage response due to unexpected (though minor) physicochemical phenomena etc. Some of these errors may also interact among themselves. Such errors cannot be easily modelled since they are not well understood or predictable. Consequently, an analytical solution for τ_1 *using actual measurements* will give multiple answers, discrimination of which to get a unique solution is impossible without additional information or arbitrary assumptions. The solutions obtained are therefore useless from a practical point of view.

For similar reasons, no simple curve fitting procedure will provide unique and acceptable solution of Equation 2 for the parameters when using actual measurements, unless the errors are modelled and suitable correction procedures are incorporated.

2.4. *A new robust data processing procedure*

What is required therefore is a robust data processing procedure, not vulnerable to the usual errors in measurements or small fluctuations in cell response, and which provides a unique, acceptable solution of Equation 2 when applied to practical cell test data. Such a procedure is proposed below.

Equation (2) shows that V against t is nonlinear. Let two instants of time t^* and t^{**} be chosen in the initial region of the V–t curve (Fig. 3) such that there is a measurable difference in the slopes of the curve (m^*, m^{**}) at these times. The slope in this region is governed by the relaxation processes at both the electrodes 1 and 2. Since the coefficients and the indices of the two exponential terms in Equation 2 have the same sign, the numerical value of the slope of the measured V–t curve is the numerical sum of the slopes of the two relaxation processes (designated as τ_1-process at electrode 1 and τ_2-process at electrode 2 henceforward) in the cell. Assuming that the faster of the two is the

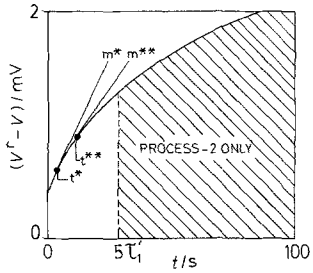

Fig. 3. Typical cell discharge transient under GNDT conditions. t^* and t^{**} are any two arbitrarily chosen points at the beginning of the transient. m^* and m^{**} are the respective slopes of these points. The vertical part of the curve at $t = 0(+)$, is generally influenced by inertial effects, switching transients and inductive spikes, and hence excluded from the analysis. The test current is of the order of $C/2000$ A where C is the nominal capacity in Ah of the battery cell under test.

τ_1-process, the steady state for the τ_1-process will be approached before that for the τ_2-process.

In order to start the analysis, the measured slopes (m^*, m^{**}) may be tentatively assigned entirely to the τ_1-process so that the value of the time constant thus calculated (τ_1') from Equation 5 is necessarily equal to, or higher than, the true value (τ_1):

$$\tau_1' = \frac{t^{**} - t^*}{\ln(-m^*) - \ln(-m^{**})} \quad (5)^*$$

Since the function $(1 - \exp(-t/\tau)$ attains 99.3% of its final (or steady state) value for $t = 5\tau$, it follows that the τ_1-process would have practically attained its steady state at $t \geqslant 5\tau_1'$.

Hence, the V–t transient at $t \geqslant 5\tau_1'$ is solely due to the τ_2-process (Fig. 3). The equation for the transient obtained from Equation 2 at $t \geqslant 5\tau_1'$ is therefore

$$V^r - V = I(R_\Omega + R_{t,1}) + IR_{t,2}(1 - e^{-t/\tau_2}) \quad (6)$$

Further

$$\ln\left(-\frac{dV}{dt}\right) = \ln\left(\frac{IR_{t,2}}{\tau_2}\right) - \frac{t}{\tau_2} \quad (7)$$

A linear plot of $\ln(-dV/dt)$ against t in the domain $t > 5\tau_1'$ will verify the existence of the τ_2-process and provide τ_2 and $R_{t,2}$ (and therefore also $C_{d,2}$) through its slope, and intercept at $t = 0$ (by extrapolation).

Substitution of these parameters in Equation 6 followed by a plot of $(V^r - V)$ against $\exp(-t/\tau_2)$ will give a straight line in the domain $t > 5\tau_1'$. The intercept at $t = 0$ obtained by extrapolation of the straight line gives the value of the total internal resistance R_i $(= R_\Omega + R_{t,1} + R_{t,2})$.

The parameters $R_{t,2}$, τ_2, $C_{d,2}$ and R_i determined above are unaffected by the assignment of the slope in the initial region of the V–t transient to τ_1-process only, since this procedure only overestimates τ_1, thereby identifying accurately the domain exclusively governed by the τ_2-process.

* Equation 5 is readily obtained by differentiating Equation 2 on ignoring the contribution of the τ_2-process (i.e., the term containing τ_2), replacing τ_1 by τ_1', and setting $t = t^*$, t^{**} successively. m $(= dV/dt)$ is negative for battery discharge.

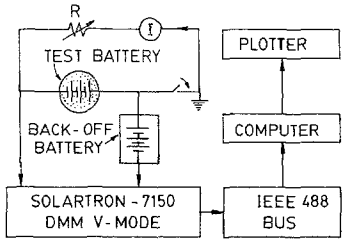

Fig. 4. Test set-up (schematic) for digital recording of V–t transient under GNDT conditions. Test battery: sealed recombinant Pb-acid battery (YUASA 6 V, 4 Ah) at SOC = 90%. DVM: SOLARTRON-7150 digital multimeter in V_{dc}-mode (200 mV range $\pm$ 10 μV resolution), R: resistance adjusted to give desired constant current when switch is closed. Back-off battery: similar to test battery, and charged to about 90% SOC, and kept on open circuit for about 50 h prior to test.

Equation 2 may now be recast as

$$Y = -IR_{t,1} \exp(-t/\tau_1) \quad (8)$$

where $Y = V^r - V - IR_i + IR_{t,2} \exp(-t/\tau_2)$.

Hence

$$\ln(-Y) = \ln(IR_{t,1}) - t/\tau_1 \quad (9)$$

Since Y is now known completely at each t, a plot of $\ln(-Y)$ against t in the domain $t < 5\tau_1'$ may be constructed which will be a straight line of slope $(-1/\tau_1)$ and intercept (at $t = 0$) of $IR_{t,1}$.

Finally, the value of τ_1 found thus may be used as a new or improved value of τ_1', and the calculations from Equation 6 onward may be repeated until the resulting parameters are constant in two successive calculations. This iterative approach is easily computerized due to the availability of digital data.

All the five parameters (R_Ω, $R_{t,1}$, $R_{t,2}$, $C_{d,1}$ and $C_{d,2}$) of the battery cell are thus determined individually, accurately and nondestructively by a momentary discharge under galvanostatic conditions.

3. Experimental aspects

The fundamental requirements of the experiment, which arise out of the GNDT conditions specified, are the accurate measurement of minute changes in battery cell voltage at short time intervals during galvanostatic discharge at an insignificant rate.

The test set up that has been successfully developed is shown in Fig. 4. A digital multimeter (Solartron 7150) used in the voltage mode (0.2 V_{dc} range, 10 μV resolution) and controlled by a computer through IEEE 488 card was used to acquire the data points correct to $\pm$ 10 μV at every 73 ms for a total duration of about 100 s. The set up was calibrated initially, with precisely known passive elements in place of the test battery, the back-off battery being unnecessary in this case, while the data obtained were processed according to the procedure described under 'theory'.

Sealed recombinant type lead-acid batteries (YUASA 6 V 4 Ah) were used for the test. Three batteries were charge–discharge cycled ($C/20$ rate charging for 22 h, discharged at the same rate to a 5.5 V cut-off) several (usually 3–4) times until a constant discharge capacity was realized. The capacity thus found was 4.0 $\pm$ 0.1 Ah at 25 $\pm$ 2°C. The batteries were then fully charged at $C/20$ rate for 22 h, discharged at $C/20$ to the desired state of charge, given an open circuit stand time of various durations (Fig. 10), and the discharge test was begun under GNDT conditions for each battery separately, by drawing a predetermined small test current (about $C/2000$ A) using the test battery itself as the source and an appropriate series resistance to control the current at the desired level i.e., without a forced discharge. The battery voltage was backed-off by a stabilized sealed 6 V lead acid battery at 90% SOC, in order to use the full sensitivity of the digital multimeter.

Considerable care was found necessary to achieve data of the required quality. Thus, the temperature coefficient of cell EMF being above -0.6 mV (deg C)$^{-1}$ [10], a temperature control of $\pm$ 0.05 °C during the test run is necessary. Thermoelectric e.m.f. and spurious corrosion-induced potentials due to bimetallic junctions were minimized by careful cleaning and drying of circuit junctions until the residual e.m.f. in a dummy circuit (without battery) was about 30 μV.

The reproducibility of the discharge transient was verified by repeating the discharge at intervals of about 45 min open circuit stand time between runs using batteries which were aged for about 50 h (to eliminate initial ageing-induced changes) at the given state of charge. The 45 min rest between successive discharge runs was found to be adequate to give a practically constant value of V^r which changed by less than 5 μV min^{-1} at the beginning of the test. The V^r value for a given discharge transient was always taken as that which prevailed at the beginning of the test.

Although the theory and the basic experimental plan is equally applicable to the charging transient of the test battery under GNDT conditions, a significant advantage accrues with the discharge transient due to the fact that, in the latter case, there is no extraneous power source in the discharge circuit described above and hence there is no distortion of the measured transient that is otherwise likely to occur.

4. Results and discussion

4.1. *Simulation test*

The test set-up and the data processing procedure were verified first by simulating the battery as per the equivalent circuit of Fig. 2 with passive elements of 0.1% accuracy. The experimental transient, and the curve theoretically calculated from the known values of circuit elements are shown in Fig. 5. The excellent agreement obtained proves the reliability of the test set up as well as that of the new data-processing procedure.

A variety of results obtained with sealed recombinant lead–acid batteries is presented below.

4.2. *Reproducibility*

In order to verify the reproducibility of test data on

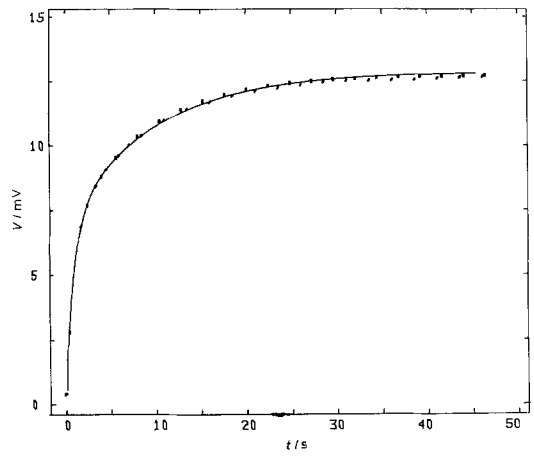

Fig. 5. Simulation test using passive elements in the battery equivalent circuit of Fig. 2. R_Ω = 10 kΩ; $R_{t,1}$ = 105 kΩ; $R_{t,2}$ = 110 kΩ; $C_{d,1}$ = 9.1 μF; $C_{d,2}$ = 99 μF. Points are from experimental measurement with a charging current I = 61 nA. Continuous line is calculated from the above parameters and Equation 2. Filled square (■) points represent the result obtained by analysis of the experimental transient by the new data-processing procedure, and recalculation of the transient with the parameters thus obtained.

repetitive scanning of the transient under GNDT conditions, two discharge runs were conducted on the same battery with a short period of open circuit stand between successive runs to attain an equilibrium state (Fig. 6). It is observed that a repetitive scanning of the transient under GNDT conditions gives identical results if the V^r value is measured at the beginning of each test run and used for calculating $(V^r - V)$.

4.3. *Linearity*

As follows from Equation 2, $V^r - V$ should depend linearly on I, or $(V^r - V)/I$ should be independent of I, if the model used and the GNDT conditions are appropriate. Figures 7 and 8 show that the $(V^r - V)/I$ (at a given t) is independent of I (within 1%) as long as the cell voltage drop $(V^r - V)$ is within about 1 mV/cell or (3 mV/battery), consistent with the requirement of linear polarization of the battery electrodes for the derivation of Equation 2. By such an experiment, however, the upper limit of the test current can be decided upon since it governs the time span of the transient usable for analysis i.e., before $(V^r - V)$ exceeds about 1 mV/cell in the present case.

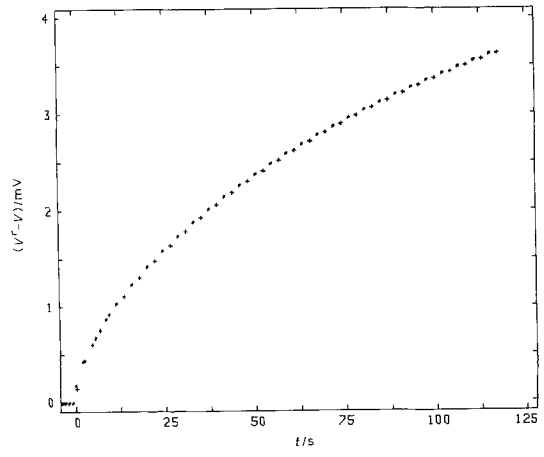

Fig. 6. Discharge transients for battery (6 V, 4 Ah SLA) during two consecutive test runs with 45 min open-circuit stand time between runs. The V^r values at t = 0(–) for the two runs are 6.37119 V, 6.37092 V and I = 1.948 mA (C/2000 rate). Temperature = 24.7 ± 0.05° C, SOC = 90%. The number of points shown in the figure is, for clarity, only about one-quarter the actual number of points obtained experimentally.

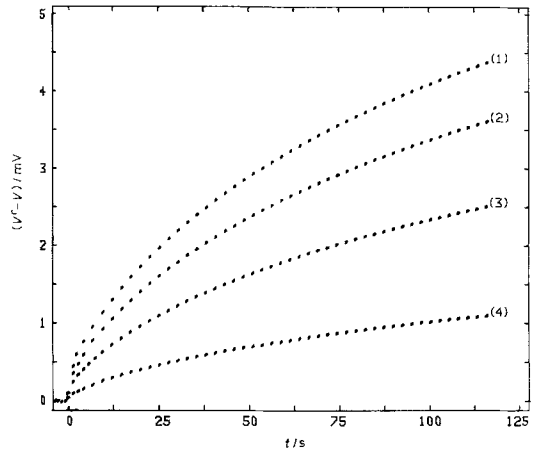

Fig. 7. Discharge transients for (6 V, 4 Ah SLA) currents: (1) 2.39, (2) 1.948, (3) 1.331 and (4) 0.569 mA. Temperature = 25.6 ± 0.1° C. SOC = 90%. The number of points shown are reduced as in Fig. 6.

The magnitude of the test current for the GNDT method is therefore important both to validate the model and to get a range of time convenient for accurate data-processing. In the present case, the test current should therefore preferably be about C/2000 A (2 mA) or less for a 125 s duration of the transient to be available for analysis, before the cell voltage falls by about 1 mV.

4.4. *Absence of diffusion control*

A confirmation of the absence of diffusion control in the initial region of the transient (t < 200 s in the present case) is obtained by plotting $(V^r - V)$ against $t^{1/2}$ (and $t^{1/3}$) over a relatively long time of discharge (Fig. 9).

The characteristic linear dependence on $t^{1/2}$ (planar diffusion model) or, on lower powers of t (porous electrode diffusion models), for diffusion-controlled condition is observed only beyond about 200 s in the present case, which justifies analysis of the data at

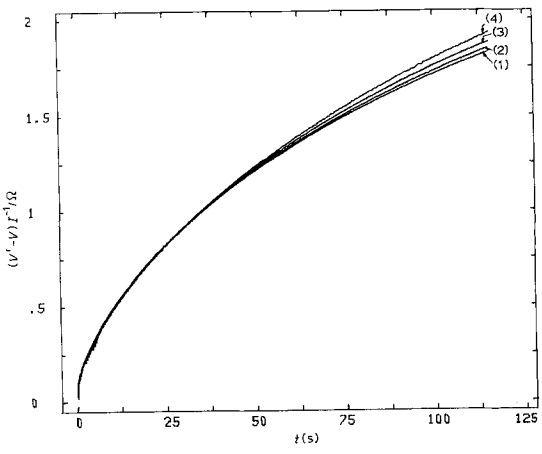

Fig. 8. $(V^r - V)/I$ against t from data in Fig. 7.

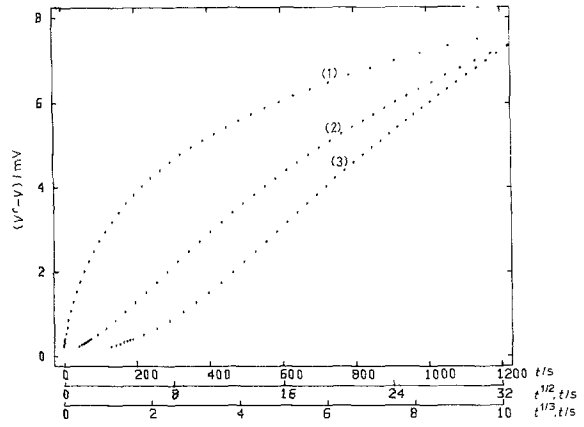

Fig. 9. Plots of $(V^r - V)$ against (1) t, (2) $t^{1/2}$ and (3) $t^{1/3}$ for battery (6 V, 4 Ah SLA) discharge under GNDT conditions. Test current 1.83 mA (about $C/2000$ A). Temperature: 23 ± 0.1°C. SOC = 90%.

$t < 200$ s according to the model proposed in this work.

Having thus identified the variables to be controlled to validate the model and the theory, a parametric characterization of batteries was made by the GNDT method as a function of open-circuit stand period of the batteries (Fig. 10) since this was found to be a significant variable. The subtle changes which occur in the battery during ageing are well reflected in the GNDT transients of Fig. 10.

4.5. *Calculations*

The data in Fig. 10 were analysed by the procedure described earlier. The value of m^* to start the calculations (Equation 5) was evaluated at the third data point (V_{iii}, t_{iii}) after $t = 0$, using the adjacent data points (V_{ii}, t_{ii}); (V_{iv}, t_{iv}) by averaging thus:

$$m^* = \frac{1}{2}\left(\frac{V_{iii} - V_{ii}}{t_{iii} - t_{ii}} + \frac{V_{iv} - V_{iii}}{t_{iv} - t_{iii}}\right)$$

The value of m^{**} was calculated similarly 1 s after the third data point, i.e., at (t_{iii} + 1). As a typical case, details of processing of curve 4 in Fig. 10 are given below.

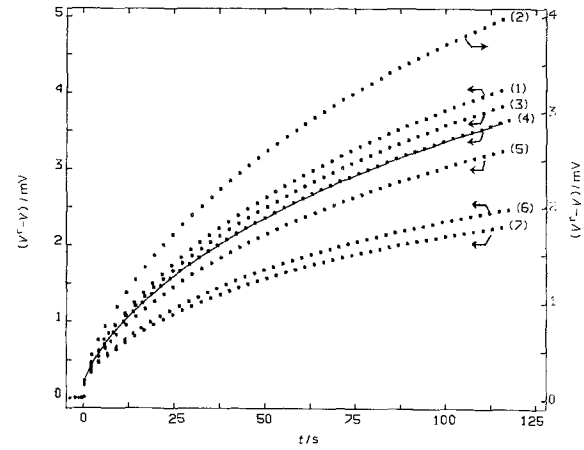

Fig. 10. Discharge transients for battery (6 V, 4 Ah SLA) at a current of 1.948 mA (about $C/2000$ rate), with open circuit stand time (prior to discharge) of: (1) 125, (2) 94, (3) 70, (4) 49, (5) 26, (6) 2 and (7) 1 h. Temperature = 24.7 ± 0.05°C. SOC = 90%. Continuous line is calculated from the parameters of the equivalent circuit evaluated by processing the data points of curve 4 following the procedure described in the text.

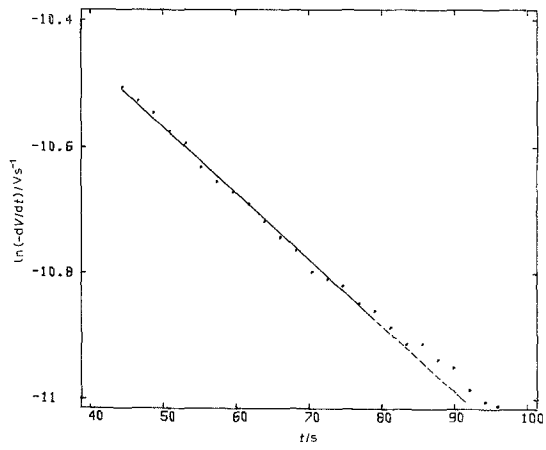

Fig. 11. Plot of ln $(-dV/dt)$ against t for curve 4 in Fig. 10 at $t > 5\tau_1'$ (τ_1' = 8.43 s for curve 4).

Using the τ_1' value (8.43 s) thus found, in the domain $t > 5\tau_1'$ a plot of ln $(-dV/dt)$ against t was constructed (Fig. 11). Derivative at each point was obtained by averaging the slopes over a short interval on either side of each chosen point.

A straight line through the points was drawn according to a least squares fit, which showed a correlation coefficient of −0.99. From the slope of the line and intercept at $t = 0$ the values of $R_{t,2}$ and τ_2 were evaluated according to Equation 7.

Next, a plot of $(V^r - V)$ against exp $(-t/\tau_2)$ was constructed in the same time domain i.e., $t > 5\tau_1'$ (Fig. 12). A straight line was drawn according to least-squares fit which gave a correlation coefficient of −0.9999. From the intercept of the line at $t = 0$, the value of $(R_\Omega + R_{t,1})$ was obtained using Equation 6. From the slope of the line, $R_{t,2}$ is obtained, which is usually more accurate than the value obtained from Fig. 11.

Finally, a plot of ln $(-Y)$ against t according to Equation 9 was constructed (Fig. 13) in the time domain $t < 5\tau_1'$. The straight line with a least squares fit gave a correlation coefficient of −0.99. From

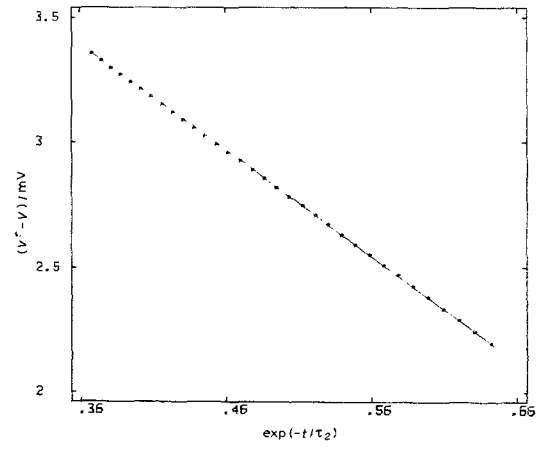

Fig. 12. Plot of $(V^r - V)$ against exp $(-t/\tau_2)$ at $t > 5\tau_1'$ from data for curve 4 in Fig. 10, τ_2 value being found from Fig. 11 and Equation 7.

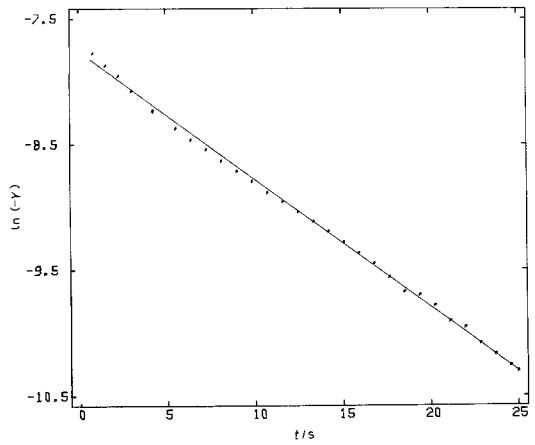

Fig. 13. Plot of ln $(-Y)$ against $t < 5\tau_1'$ from data for curve 4 in Fig. 10. The Y value is calculated from parameters obtained in Fig. 12 and Equation 8.

the slope and intercept of the line, $R_{t,1}$ and τ_1 were evaluated.

Using the value of τ_1 thus found as an improved value of τ_1', calculations were repeated until the parameters converged to within $\pm 2\%$. This required usually just 7 iterations.

The entire calculations described above were carried out with a software programme written in Quick-BASIC. Data of V against t from a GNDT experiment could thus be processed on a PC in a few seconds, since the data were acquired and stored in digital form, correct to $\pm 10\,\mu$V at intervals of 73 ms for first 5 s and correct to $\pm 1\,\mu$V at intervals of 0.4 s, subsequently.

As a final check, the impedance parameters of the battery thus obtained ($R_\Omega = 0.125\,\Omega$; $R_{t,1} = 0.200\,\Omega$; $R_{t,2} = 2.090\,\Omega$; $C_{d,1} = 42.16$ F; $C_{d,2} = 43.57$ F; for curve 4 in Fig. 10.) were inserted into Equation 2, and the V–t transient was calculated at $I = 1.948$ mA. A comparison of this curve with experimental data (Fig. 10) shows the excellent agreement obtained, justifying the entire procedure.

4.6. *Impedance parameters*

Figure 14 summarizes the impedance parameters thus obtained for all the curves in Fig. 10. It may be noticed that the double layer capacitances and charge transfer

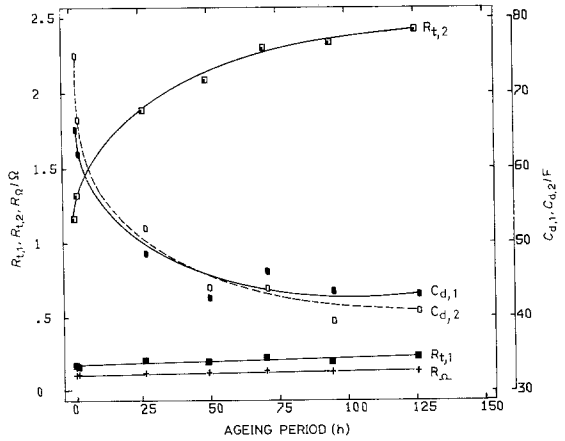

Fig. 14. Plot of impedance parameters calculated from Fig. 10 against ageing period.

resistances of the cathode and anode of the battery have been obtained separately, perhaps for the first time, in addition to the ohmic part of the internal resistance of the battery.

The assignment of the cathode and anode, however, is, as yet, arbitrary. In other words, whether the subscripts 1 and 2 represent cathode and anode, or anode and cathode, requires to be resolved by additional considerations in future.

Nevertheless, interesting conclusions may be drawn from the data in Fig. 14. The double layer capacitances $C_{d,1}$ and $C_{d,2}$ fall fairly steeply in the first few hours of ageing, and reach nearly constant, equal values after about 100 h of ageing period at a 90% state of charge battery. This reflects, perhaps, on crystal growth-induced area shrinkage at the two electrodes. The charge transfer resistances, on the other hand, show different trends, $R_{t,2}$ rising relatively rapidly in the first few hours of ageing as compared to $R_{t,1}$ which remains nearly constant all through. Moreover, the steady state value of $R_{t,2}$ is fairly large, being about 2.4 Ω, while the total internal resistance obtained by conventional methods (and therefore, relatively destructive tests) is a few tenths of an ohm for these batteries [11]. These facts indicate the presence of a labile film on the electrode corresponding to $R_{t,2}$, the film being readily broken down at normal discharge rates of $C/20$ or higher, but is regenerated on open circuit stand. The susceptibility to form a film is more likely with spongy lead electrode due to open circuit corrosion and formation of a thin $PbSO_4$ film than with the PbO_2 electrode. This suggests that $R_{t,2}$ corresponds to the Pb anode and $R_{t,1}$ to the PbO_2 cathode. It may then be inferred that a further improvement of the battery is to be sought primarily by reducing $R_{t,2}$, i.e., by electrocatalysis of the lead anode. Finally, the constant small value of R_Ω shows that the separator design and electrolyte distribution are already at an optimal level in the starved-electrolyte type sealed battery.

5. Conclusions

A new technique has been proposed for the non-destructive determination of the resistance and reactance parameters of cathodes as well as of anodes separately in sealed battery cells. The technique allows some key developments.

1. The model and data-analysis are not restricted either to linear approximations in the time domain or to well ordered data. The nonlinear-in-time model retains all the important impedance parameters of real systems while the data analysis leads logically to unique and reliable values of the electrode impedance parameters and cell internal resistance, from measurements on real systems.

2. The diffusion impedance which usually distorts the data and complicates the analysis has been rendered negligible by adopting suitable (and verifiable) test conditions.

3. Effects due to any series inductance of battery

cells, which render AC impedance measurements of doubtful value, have been eliminated by the galvanostatic test mode.

4. Switching transients have no effect on the results since the data made use of for analysis are those obtained well after the decay of these transients.

5. The technique provides for the first time a fundamental framework for the evaluation, design-improvement, and development strategies for battery systems since the impedance parameters are obtained as discrete contributions from cathode, anode and the electrolyte/separator components of sealed batteries.

Extension of this work to determine the impedance parameters of individual electrodes as a function of state of charge of lead–acid, nickel–cadmium, zinc–manganese dioxide and lithium-based batteries is in progress.

Acknowledgements

The authors thank the Council of Scientific & Industrial Research, New Delhi for financial support to SAI.

References

[1] P. R. Roberge, E. Halliop, G. Verville, J. Smit, *J. Power Sources* **32** (1990) 261.
[2] B. Savova-Stoynov, Z. B. Stoynov, *J. Appl. Electrochem.* **17** (1987) 1150 and references therein.
[3] S. Sathyanarayana, S. Venugopalan, M. L. Gopikanth, *ibid.* **9** (1979) 125.
[4] M. L. Gopikanth, S. Sathyanarayana, *ibid.* **9** (1979) 369.
[5] M. Hughes, R. T. Barton, S. A. G. R. Karunathilaka, N. A. Hampson, *ibid.* **15** (1985) 129.
[6] I. Epelboin, M. Keddam, H. Takenouti, *ibid.* **2** (1972) 71.
[7] F. Gutmann, *J. Electrochem. Soc.* **112** (1965) 94.
[8] S. Okazaki, S. Higuchi, N. Kubota, S. Takahashi, *J. Appl. Electrochem.* **16** (1986) 513.
[9] S. R. Narayanan, S. Sathyanarayana, *J. Power Sources* **24** (1988) 295.
[10] H. Bode, 'Lead-Acid Batteries', (translated by R. J. Brodd and K. V. Kordesch), John Wiley and Sons, New York (1977).
[11] 'Application Manual', Yuasa Battery Co. Ltd, Tokyo, Japan (1987), p. 10.